Supplementary Information for

Rcf2 revealed in cryoEM structures of hypoxic isoforms of mature mitochondrial III-IV supercomplexes

Andrew M. Hartley, Brigitte Meunier, Nikos Pinotsis, Amandine Maréchal

Corresponding author: Amandine Maréchal
Email: a.marechal@ucl.ac.uk

This PDF file includes:

Supplementary text
Figures S1 to S6
Table S1

Supplementary Information Text

Atomic model building for Rcf2

The additional density present in CIV resembled a TM-helix-loop-TM-helix motif, a motif that is found in both Rcf1 and Rcf2, two proteins implicated with roles in SCs. To assign the correct protein to this additional density, we aligned the Rcf1 and Rcf2 sequences using Clustal Omega (1). We then manually adjusted the alignment by taking into account the transmembrane helices of Rcf1 and Rcf2 as predicted by HMMTOP (2) and TMHMM (3) (*SI Appendix*, Fig. S5*A*, predicted transmembrane helices are highlighted in yellow). Two polyalanine models were then built into the density covering both chain directions. The Cβ positions allowed us to locate three bulky side chain densities within one of the TM α-helices. These were modelled as W-x-x-x-x-Y-x-x-W, a sequence found only within a predicted TM domain on Rcf2 (W124-Y129-W132, highlighted with asterisks under the sequence). Two other tryptophans at the N-terminus of Rcf2 (W52 and W59, triangles) were ruled out as possible candidates because they are only seven residues apart and cannot fit into the density as a helix, and lack a third bulky residue to fill the density that we assigned to Tyr129.
Rcf1 also contains two tryptophan residues which are eight positions apart (W58 and W66, filled circles), however these were excluded for two reasons; (i), they are not within a predicted transmembrane region of the protein, and (ii), each tryptophan is flanked by either two lysines or two arginines (*SI Appendix*, Fig. S5*A*), and there is clearly no density in the map to support the presence of long side chain residues around them (see densities around W124 and W132 in *SI Appendix*, Fig. S5*B*).
Furthermore, large sequences of Rcf2 fit well into the density of the two transmembrane helices, as demonstrated by the side chain densities of Trp124-Val135 and Ile147-Thr158, while no similar sequences exist in Rcf1 (*SI Appendix*, Fig. S5*A,B,C*). The final model of Rcf2 satisfies electrostatic and hydrophobic interactions which are shown in Fig. 4, including interactions of the QQRQ motif with other CIV subunits, allowing us to conclude with confidence that Rcf2 is the additional protein present in the map.
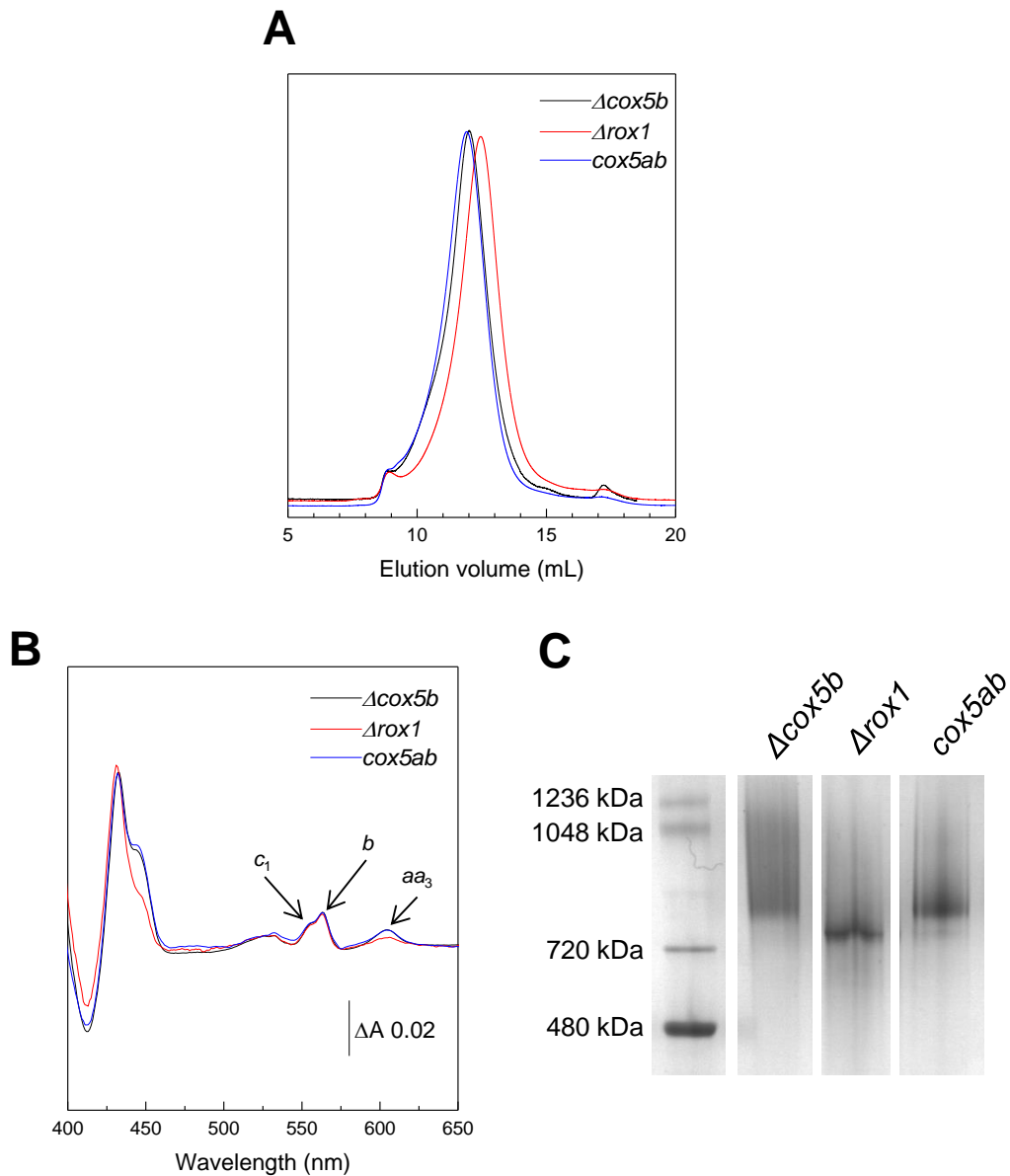
A

B

C

Fig. S1. Purification of III-IV SCs from *Δcox5b, Δrox1* and *cox5ab*. (*A*). Gel filtration elution profile of metal-affinity purified III-IV SCs from all three *S. cerevisiae* mutant strains. The peak fraction was used for cryoEM sample preparation. (*B*). Reduced *minus* oxidised visible absorption spectra recorded on purified III-IV SCs. The absorption bands specific to cyt aa_3 of CIV (445 and 604 nm), cyt *b* of CIII (432 and 562 nm) and cyt c_1 CIII (554 nm) are indicated with arrows. Traces are normalised on their $\Delta A_{562-578nm}$. (*C*). BN-PAGE gel of the purified III-IV SCs.

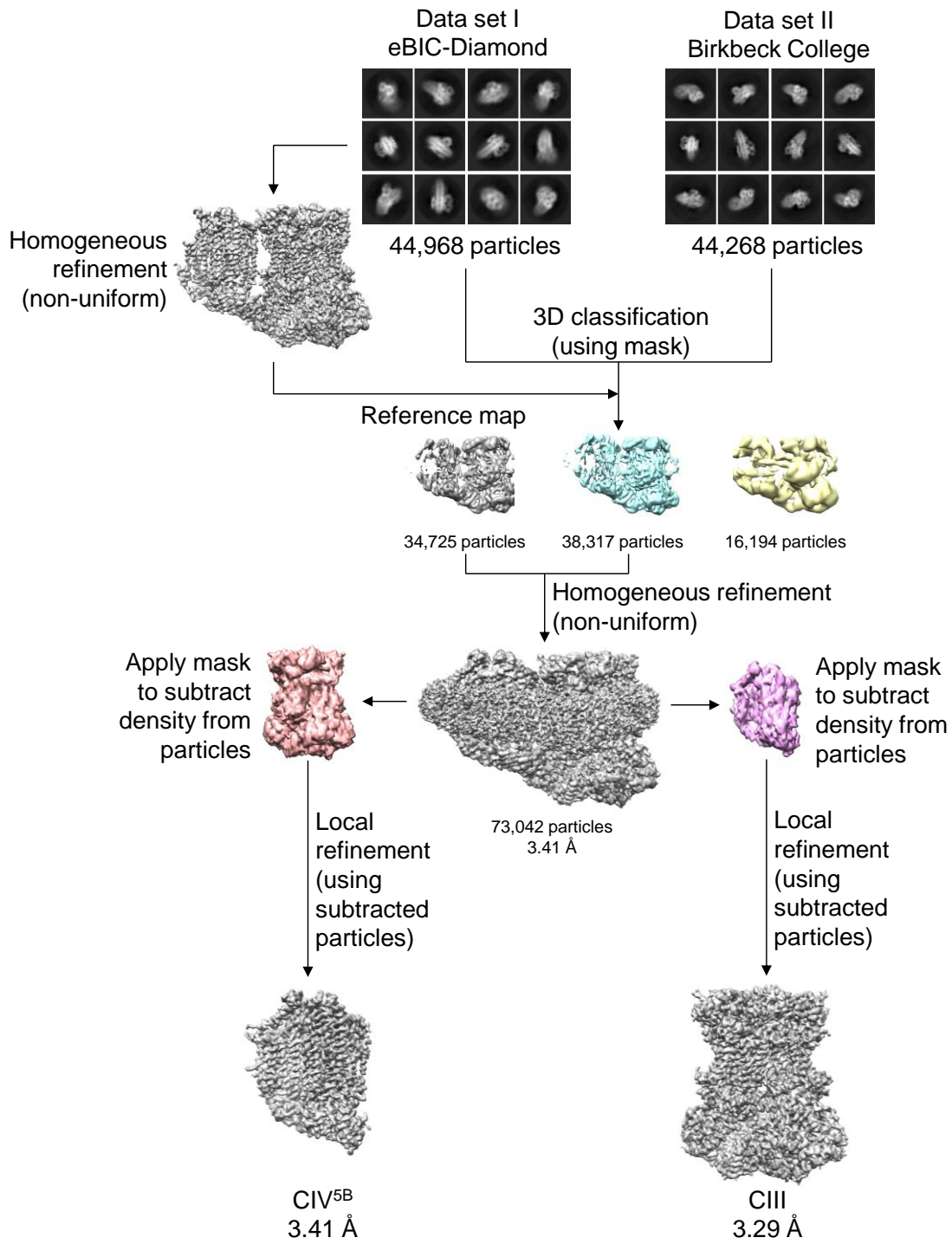**Fig. S2. Cryo-EM data workflow of 3D classification and focussed refinement for the III$_2$-IV$^{5B}_1$ SC purified from *Δrox1*.**
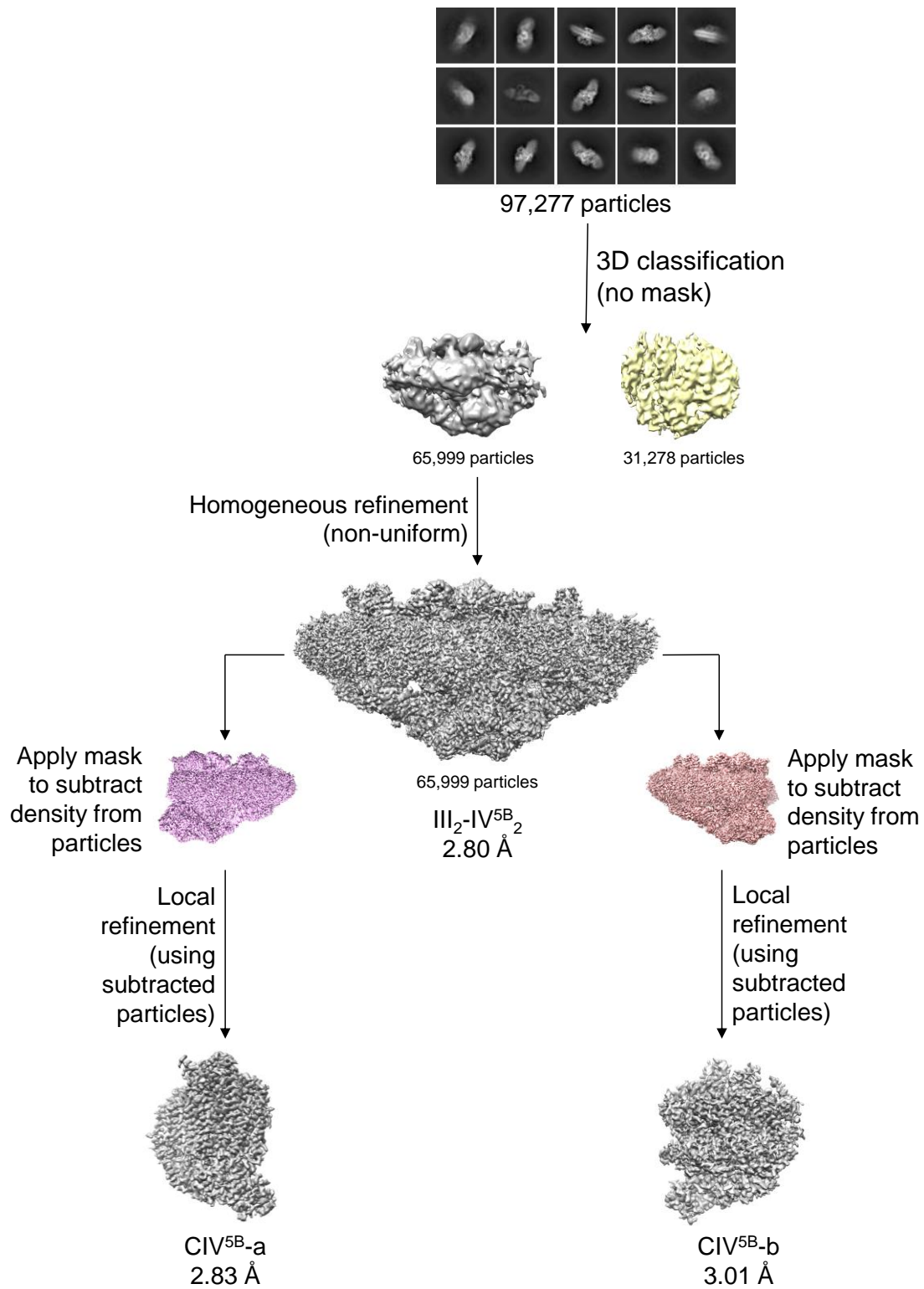
Fig. S3. Cryo-EM data workflow of 3D classification and focussed refinement for the III_2-IV^{5B}_2 SC purified from $\Delta cox5ab$.
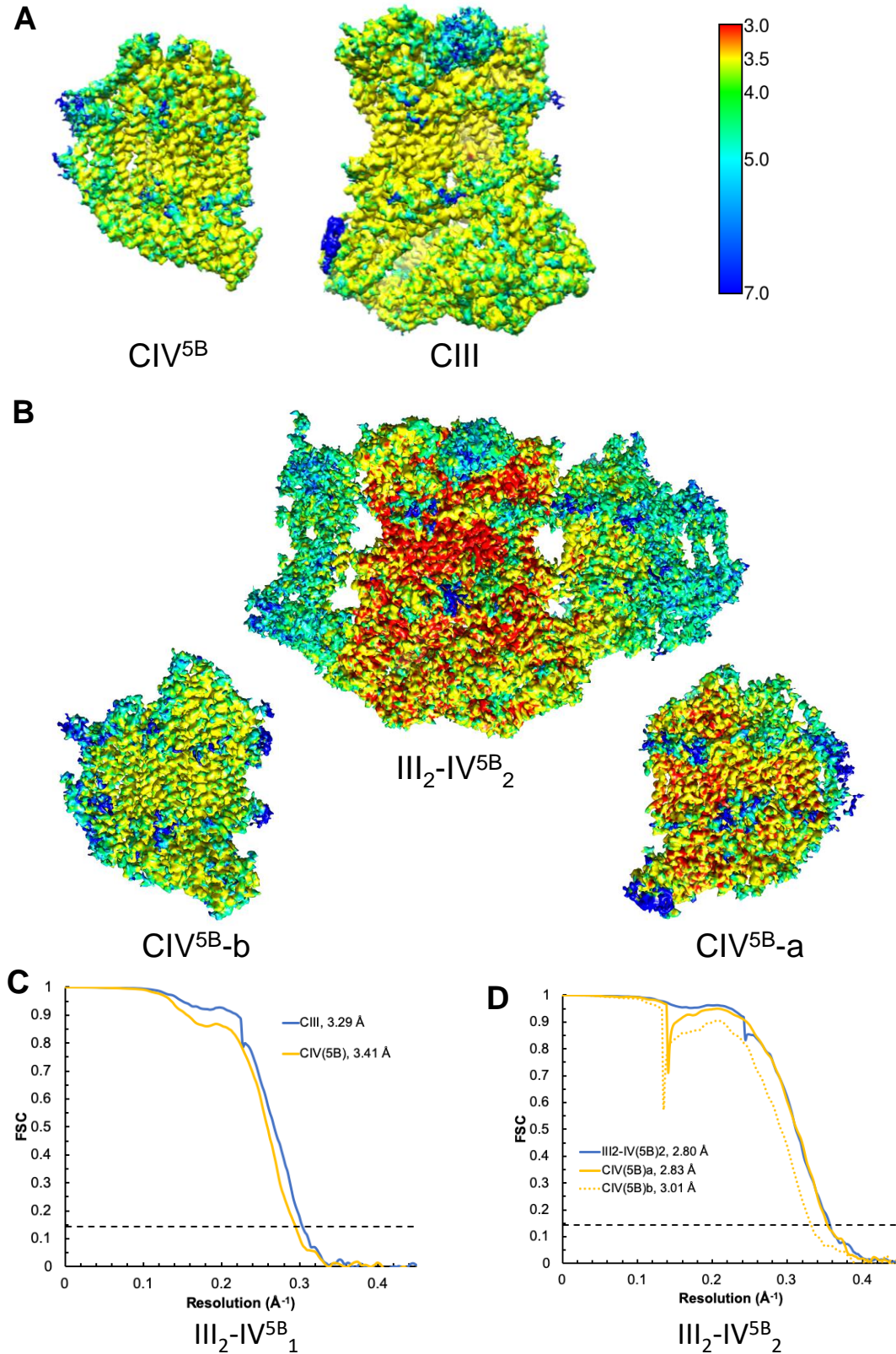
Fig. S4. Final cryoEM maps obtained after focus refinement on the two CIV^{5B}-containing SCs. Surface rendering maps are coloured according to local resolution for (*A*), CIII and CIV^{5B} within the III$_2$-IV$^{5B}_1$ SC purified from *Δrox1* and (*B*), the III$_2$-IV$^{5B}_2$ SC obtained after homogeneous refinement and its two CIV^{5B} (-b and -a) after focus refinement. Fourier shell coefficient (FSC) curves for each map are presented in (*C*), for CIII and CIV^{5B} within the III$_2$-IV$^{5B}_1$ SC and (*D*), for III$_2$-IV$^{5B}_2$ and CIV^{5B}-a and -b within the III$_2$-IV$^{5B}_2$ SC.

A

```
RCF2_YEAST,  MKILTQDEIEAHRSHTLKGGIEGALAGFAISAIIFKVLPRRYPKFKPSTLTWSIKTALWITPPTVLTAIC    70
RCF1_YEAST,  ------------------------------------------------------------------MS     2
                                                                      Δ       Δ
                                               α1        α2
RCF2_YEAST,  AEEASNNFDATMYGSGSSSEDALDEHRRWKSLSTKDKFVEGLSNNKYKIIT--GAWAASLYGSWVIVNKD   138
RCF1_YEAST,  RMPSS--F---------DVT-----ERDLDDMTFGERIIYHCKKQPLVPIGCLLTTGAVILAAQNVRLGN    56
                                                                *      *  *
                    α3                                    α4
RCF2_YEAST,  PIMTKAQKIVQARMYAQFITVGLLLASVGLSMYENKLHPNKQKVN-------EMRRWENALRVAEEEER   200
RCF1_YEAST,  --KWKAQYYFRWRVGLQAATLVALV--AGSFIYGTSGKELKAKEEQLKEKAKMREKLWIQELERREEETE   122
                  •      •
RCF2_YEAST,  LEKE---GRRTGYVSNEERINSK---------IFKS   224
RCF1_YEAST,  ARRKRAELARMKTLENEEEIKNLEKELSDLENKLGKK   159
```

B

Ala123 Trp124 Ala125 Ala126 Ser127 Leu128

Tyr129 Gly130 Ser131 Trp132 Val133 Ile134 Val135

C

Ile147 Val148 Gln149 Ala150

Arg151 Met152 Tyr153 Ala154

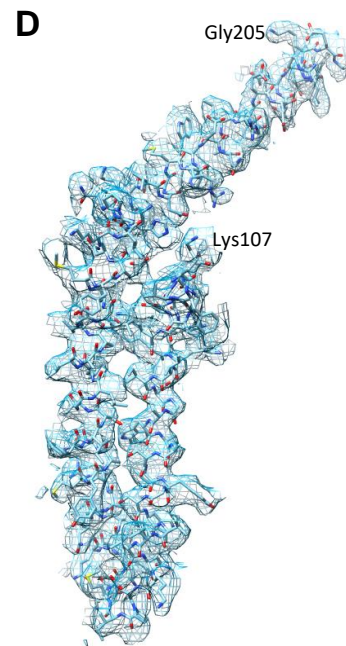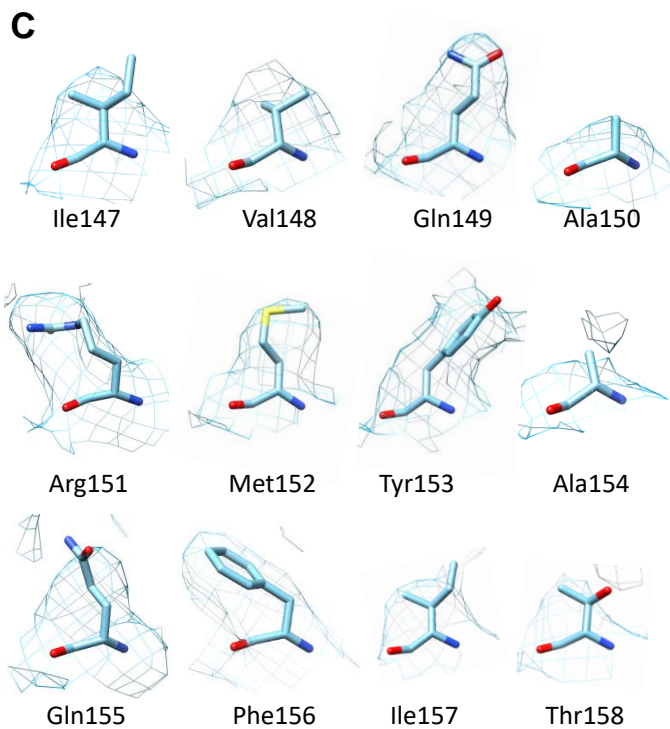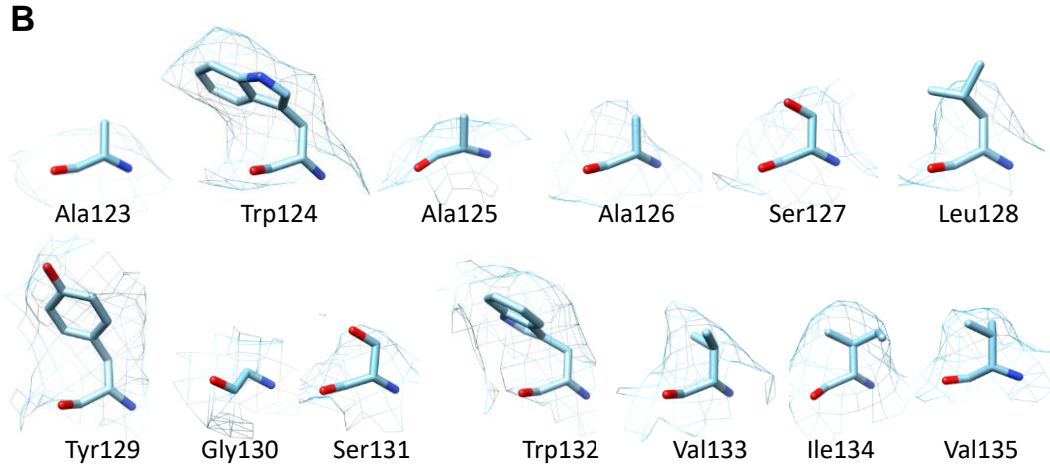Gln155 Phe156 Ile157 Thr158

D

Gly205

Lys107

Fig. S5. Evidence for the assignment of Rcf2 in the refined EM map of CIV^{5B} within the Δrox1 III2-IV1 SC. (*A*) Sequence alignment of Rcf2 and Rcf1 with their Q(Q/R)RQ motif in bold. The predicted transmembrane helices are highlighted in yellow. The red cylinders above the sequences highlight the α-helices assigned to Rcf2 from the electron density. Triangles and stars (Rcf2) or filled circles (Rcf1) beneath the sequences highlight the positions of tryptophan residues that were used as a starting point for tracing the amino acid sequence (see *SI Appendix*, supplementary text). Underlined amino acids refer to the densities shown in the following two panels. (*B*) Coulomb potential maps for the individual Rcf2 residues 123-135 and (*C*) 147-158. (*D*) Coulomb potential map for the entire Rcf2 fragment found in the III$_2$-IV$_1^{5B}$ SC.

A CIV^{5B}, *Δrox1*

cox5ab

B CIV^{5B}-a

C CIV^{5B}-b

D CIV^{5A}, *Δcox5b*

Δcox5b
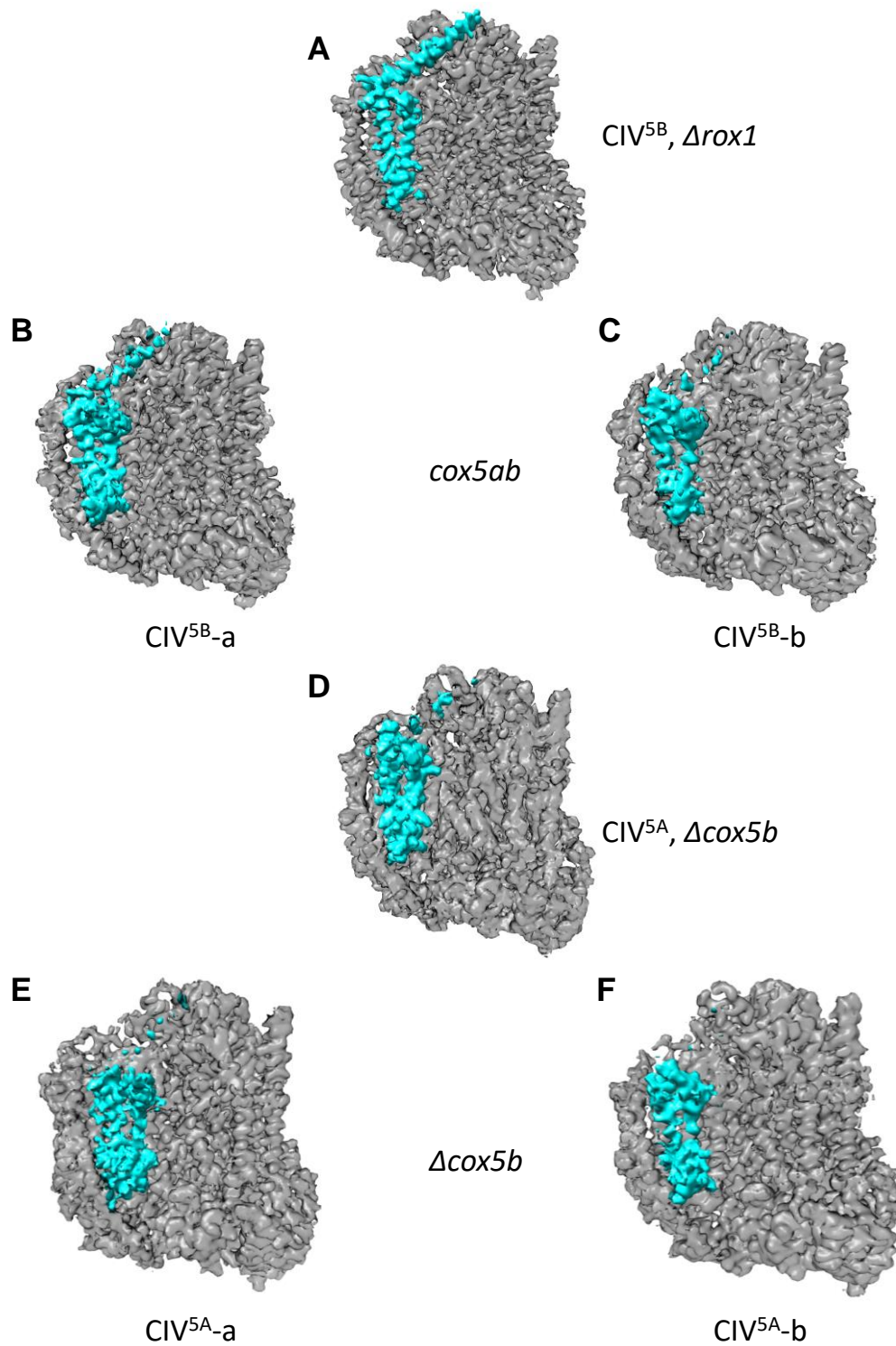
E CIV^{5A}-a

F CIV^{5A}-b

Fig. S6. Additional density observed on CIV within the different III-IV SCs. Cryo-EM maps obtained for CIV after focussed refinement. The 12 expected subunits constitutive of CIV are coloured in grey and the addition density assigned to a Hig1 type 2 protein is highlighted in cyan. (*A*) CIV^{5B} within the III$_2$-IV$^{5B}_1$ SC of *Δrox1*. (*B*) and (*C*), CIV^{5B}-a and CIV^{5B}-b within the III$_2$-IV$^{5B}_2$ SC of *cox5ab*. (*D*) CIV^{5A} within the III$_2$-IV$^{5A}_1$ SC of *Δcox5b*. (*E*) and (*F*), CIV^{5A}-a and CIV^{5A}-b within the III$_2$-IV$^{5A}_2$ SC of *Δcox5b*.

Table S1. Cryo-EM data collection, refinement and validation statistics.

Reconstruction	$\Delta rox1$ III$_2$-IV$^{5B}_1$ (PDB 6T15)		$cox5ab$ III$_2$-IV$^{5B}_2$ (PDB 6T0B)			$\Delta cox5b$ III$_2$-IV$^{5a}_2$	
	CIII (EMD-10317)	CIV^{5B} (EMD-10318)	III$_2$-IV$^{5B}_2$ (EMD-10340)	CIV^{5B}-a (EMD-10335)	CIV^{5B}-b (EMD-10334)	CIV^{5A}-a (EMD-10375)	CIV^{5A}-b (EMD-10376)
Data collection and processing							
Magnification	130,000		81,000			130,000	
Voltage (kV)	300		300			300	
Electron exposure (e$^-$/Å^2)	1.410 and 1.285		0.95			1.645	
Defocus range (µm)	-1.6 to -3.6 and -1.5 to -2.7		-1.5 to -2.8			-1.6 to -3.6	
Pixel size (Å)	1.048		1.085			1.048	
Symmetry imposed	C1		C1			C1	
Initial particle images (no.)	89,236		138,154			98,968	
Final particle images (no.)	73,042		65,998			44,194	
Map resolution (Å)	3.29	3.41	2.80	2.83	3.01	3.09	3.24
FSC threshold	0.143						
Map sharpening B factor (Å^2)	95.1	103.3	67.1	64.5	66.5	76.8	78.0
Refinement[1]							
Initial model used (PDB code)	6HU9						
Model resolution (Å) [2]	3.40		3.10				
d99 (masked, Å) [2]	3.16		2.93				
FCS model 0.5 (Å) [2]	3.52		3.06				
Map CC (masked) [2]	0.7332		0.8273				
Model composition							
Nonhydrogen atoms	48,970		64,482				
Protein residues	6,002		7,902				
Ligands and cofactors	14		22				
Lipids	31		41				
B factors (Å^2)							
Protein + ligand average	126.9		98.1				
Lipid average	124.5		73.2				
R.m.s. deviations							
Bond lengths (Å)	0.005		0.012				
Bond angles (°)	1.080		1.288				
Validation[3]							
MolProbity score	1.71		1.74				
Clashscore	5.39		5.87				
Poor rotamers (%)	0.28		0.30				
Ramachandran plot							
Favored (%)	93.65		93.66				
Allowed (%)	6.30		6.21				
Disallowed (%)	0.05		0.13				

[1.] The models were refined against a map generated by merging the maps from the 3D refinement (CIII and CIV^{5B} for $\Delta rox1$ III$_2$-IV$^{5B}_1$; III$_2$-IV$^{5B}_2$ and CIV^{5B}-a and CIV^{5B}-b for $cox5ab$ III$_2$-IV$^{5B}_2$).
[2.] Determined by phenix.mtriage
[3.] Determined by phenix.molprobity

9

SI References

1. F. Sievers *et al*., Fast, scalable generation of high-quality protein multiple sequence alignments using Clustal Omega. *Mol. Syst. Biol.* **7**, 539 (2011).
2. G. E. Tusnády, I. Simon, The HMMTOP transmembrane topology prediction server. *Bioinformatics* **17**, 849-850 (2001).
3. A. Krogh, B. Larsson, G. Von Heijne, E. L. Sonnhammer, Predicting transmembrane protein topology with a hidden Markov model: application to complete genomes. *J. Mol. Biol.* **305**, 567-580 (2001).